Wave Function Spectroscopy in Quantum Wells with Tunable Electron Density

G. Salis,[1] B. Graf,[2] and K. Ensslin[1,2]
[1]*Solid State Physics Laboratory, ETH Zürich, 8093 Zürich, Switzerland*
[2]*Paul Scherrer Institute, 5232 Villigen PSI, Switzerland*

K. Campman, K. Maranowski, and A. C. Gossard
Materials Department, University of California, Santa Barbara, California 93106
(Received 29 May 1997)

We present a new approach to investigate quantum-mechanical probability density distributions of electrons in a screened wide potential well, based on low-temperature magnetotransport measurements. Differences of subband energy levels shifted by an inserted controlled potential perturbation are measured and used to extract the difference of the squared amplitude of the respective wave functions at the location of the potential spike. The position of the wave functions and the carrier density can be tuned independently via front- and back-gate voltages. We find excellent agreement between the measured data and self-consistently calculated wave functions. [S0031-9007(97)04818-7]

PACS numbers: 73.20.Dx, 73.50.Yg, 73.61.Ey

Spectroscopy of electron states in artificial model structures is at the heart of quantum mechanics. Wave functions of intentionally modified surface states have been probed using the scanning tunneling microscope [1]. In a different approach, the energy shift of quantized states due to an inserted, highly localized potential perturbation was measured. In this way, wave functions of electrons confined in semiconductor quantum wells [2] and in surface states of metals [3] have been investigated.

Semiconductor quantum wells are generally realized in $Al_xGa_{1-x}As/GaAs$ heterostructures. Based upon the high degree of perfection achieved with molecular beam epitaxy, it is possible to realize a large variety of conduction and valence band profiles in the growth direction of semiconductor heterostructures. In particular, so-called parabolic quantum wells (PBW) have attracted a lot of attention because they can be used for unique experiments inaccessible to other potential shapes. Once filled with electrons via modulation doping [4,5], transport experiments confirm that the screened potential approximates a square well whose single particle energy levels can be probed [6].

In contrast, spectroscopy of energy levels of a screened PBW is not possible with optical intersubband transmission experiments, because the equidistant energy levels of a bare parabolic potential are measured, as if there was no electron-electron interaction [7,8]. This striking observation was explained by the generalized Kohn's theorem [9]. With a potential spike inserted into the PBW, the single line of the collective intersubband transitions splits, which is explained in terms of resonant tunnel processes [10].

In order to probe probability densities with interband optical transitions in Ref. [2], the conduction band as well as the valence band states had to be considered, and the probability density distribution of electrons and holes was assumed to be equal. Additional complications result from light-hole and heavy-hole transitions.

In this paper, we demonstrate that differences of one-electron probability density distributions of PBWs in the presence of electron screening can be probed by magnetotransport measurements. This paper is organized as follows: After presenting the concept of wave function probing, we briefly describe the measured samples and the experimental details. The method is then used to extract the difference of electron probability density distributions of two occupied subbands in the PBW for different electron sheet densities. We proceed by comparing the experimental results with self-consistent band structure calculations, which are in excellent agreement. Finally, we discuss restrictions in the applicability of the presented method.

The concept introduced in Ref. [2] is straightforward: A potential perturbation $V\delta(z - z_0)$ at the position z_0 within the PBW shifts the quantum-mechanical eigenstates $\psi_i(z)$ with energies E_i in first-order perturbation theory as

$$E_i' = E_i + V|\psi_i(z_0)|^2. \quad (1)$$

Measuring the shifted energies on many samples with different spike positions z_0 and comparing them to an unperturbed sample, the probability density distribution $|\psi_i(z_0)|^2$ for different subbands i was mapped out in Ref. [2]. In our samples, the spike position is fixed. The electron distribution itself can be displaced along the growth direction with respect to the spike by applying electric fields across the parabola. Because of the unique property of a parabolic potential that the curvature of the potential remains unaffected by the superposition of a linear electric field, the wave functions are merely displaced, and the unaltered shape of the spatially shifted wave functions can be probed at one spike position in the same sample. Obviously, this statement remains valid in the presence of electron screening.

Here we determine the single-particle energies of the screened PBW by measuring Shubnikov–de Haas

 0031-9007/97/79(25)/5106(4)$10.00

(SdH) oscillations of the longitudinal resistivity. The frequencies of the SdH oscillations yield the electron densities N_i of the occupied subbands. Based on the energy independent density of states $D = m^*/\pi\hbar^2$ of a two-dimensional system (m^* = effective electron mass), one obtains the difference of the Fermi energy E_F to the respective subband energy level E_i'. In order to eliminate E_F, which itself depends on the subband energy levels, one subtracts two subband densities, N_i and N_j. Therefore, transport experiments measure differences of subband energies $\Delta_{i,j}E' = E_i' - E_j' = \frac{\pi\hbar^2}{m^*}(N_j - N_i)$. According to Eq. (1), the influence of the potential spike is then written as $\Delta_{i,j}E' = \Delta_{i,j}E + V\Delta_{i,j}|\psi|^2$, with $\Delta_{i,j}|\psi|^2 := |\psi_i(z_0)|^2 - |\psi_j(z_0)|^2$. We obtain $\Delta_{i,j}|\psi|^2$ by comparing energy differences of two samples a and b with different spike strengths V_a and V_b:

$$\Delta_{i,j}|\psi|^2 = \frac{\Delta_{i,j}E'(V_a) - \Delta_{i,j}E'(V_b)}{V_a - V_b}. \qquad (2)$$

The denominator $V_a - V_b$ is a well known growth parameter. With this approach we have developed a method to measure differences in probability densities of occupied conduction band sublevels, based on low temperature magnetotransport experiments.

We have grown a set of four different samples similar to those described in Ref. [10]. In all of them, the PBW is realized as a 760 Å wide $Al_xGa_{1-x}As$ layer with x varying parabolically between 0 and 0.1 [11]. The well is embedded in 200 Å undoped $Al_{0.3}Ga_{0.7}As$ spacer layers with symmetric remote Si doping on both sides. The back gate is a 250 Å thick n^+-doped layer located 1.35 μm below the well, separated by 0.5 μm of low-temperature grown GaAs [12]. A TiPtAu front-gate electrode was evaporated on top of the structure. The two gates allow independent tuning of the carrier density and the position of the electron distribution inside the well. The experiments were done in standard Hall-bar geometries.

In sample 1, the unperturbed parabolic potential is realized. In each of the samples 2 to 4, a three-monolayer thick $Al_xGa_{1-x}As$ potential spike was inserted in the center of the PBW, with $x = 0.05$, 0.1, and 0.15, respectively. The spikes are described by $V\delta(z - z_0)$, where V denotes the potential height times the width of the spike. With a spike width of 8.5 Å and a potential height of $x \times 790$ meV, we have $V = x \times 6720$ Å meV. These potential perturbations are weak enough to be treated in first-order perturbation theory for $x \leq 0.15$.

Magnetotransport measurements were carried out in a He^3/He^4 dilution refrigerator at about 100 mK. The electron density can be varied between 1 and 5×10^{15} m^{-2} by applying voltages V_{fg} and V_{bg} between the electron gas and the front- and back-gate electrodes, respectively. Typical electron mobilities are about 15 m^2/V s, as obtained from the resistance at zero magnetic field. SdH-oscillations can typically be observed above 0.2 T.

Here we concentrate on the case of two occupied subbands. For the realization of our experimental idea, we have displaced the electron distribution inside the well by applying appropriate gate voltages, keeping the Hall density N_H, as obtained from the low-field Hall effect, constant.

In Fig. 1, contour lines of constant N_H in the V_{fg}-V_{bg} plane are shown for sample 2. SdH oscillations were measured for magnetic fields between 0 and 1.2 T for each pair of V_{fg} and V_{bg} along a line of constant N_H (symbols in Fig. 1). The subband density N_0 of the ground state can be evaluated with best accuracy from Fourier transformation. The density N_1 is determined using $N_1 = N_H - N_0$. The difference of probability density $\Delta|\psi|^2 := \Delta_{0,1}|\psi|^2$ in Eq. (2) is then proportional to differences of N_0, measured at the same N_H on two samples with different spikes V_a and V_b,

$$\Delta|\psi|^2 = 2\frac{\pi\hbar^2}{m^*}\frac{N_0(V_b) - N_0(V_a)}{V_a - V_b}. \qquad (3)$$

Figure 2 presents measurements of N_0 at $N_H = 2.4 \times 10^{15}$ and 3.9×10^{15} m^{-2} for samples 1 to 4. Distinct minima in N_0 are visible, which get more pronounced for larger spike strength x. The difference in N_0 for

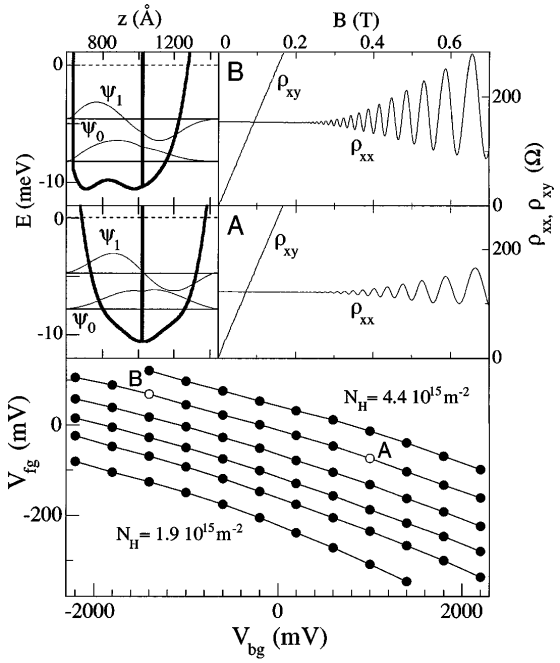

FIG. 1. Lower part: Measured contours of constant Hall density N_H for sample 2. The dots correspond to front- and back-gate voltages, V_{fg} and V_{bg}, as applied in the experiment. Upper left part: Calculated wave functions ψ_0 and ψ_1, the corresponding subband energies (straight lines), the Fermi energy (dashed lines) and the screened potential at $N_H = 3.9 \times 10^{15}$ m^{-2} for a symmetric situation (A) and with the wave functions shifted to the left (B). In the upper right part, measured magnetoresistivities ρ_{xx} and Hall resistivities ρ_{xy} are displayed for the two sets of gate voltages (A) and (B), with same Hall densities but displaced electron distributions.

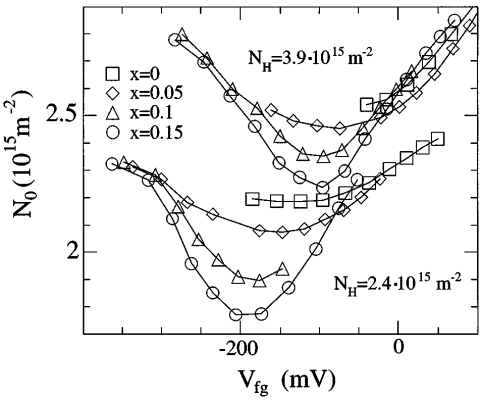

FIG. 2. Measured subband density N_0 as functions of $V_{\rm fg}$ for $N_{\rm H} = 2.4 \times 10^{15}$ and 3.9×10^{15} m^{-2} and for samples 1 to 4 (spikes with Al content $x = 0.0$, 0.05, 0.10, and 0.15, respectively, from top to bottom). The minima in N_0 are due to the potential spike. The difference of two curves at equal sheet density is directly proportional to $\Delta|\psi|^2$.

two samples with different spikes is smaller at higher densities. This is due to the fact that the width of the wave functions increases with density leading to a reduced amplitude of the wave functions at the spike positions.

According to Eq. (3), the measured data of N_0 shown in Fig. 2 can be used directly to plot $\Delta|\psi|^2$ as a function of the gate voltages. For this purpose, the data in Fig. 2 was interpolated in order to subtract subband densities of different samples. The central result is shown in Fig. 3, where all combinations of data from samples 2, 3, and 4 are shown (symbols) for two different Hall densities.

In order to obtain the spatial dependence of the measured $\Delta|\psi|^2$, it is necessary to know the relative displacement, Δz, of the electron distribution at constant $N_{\rm H}$ as

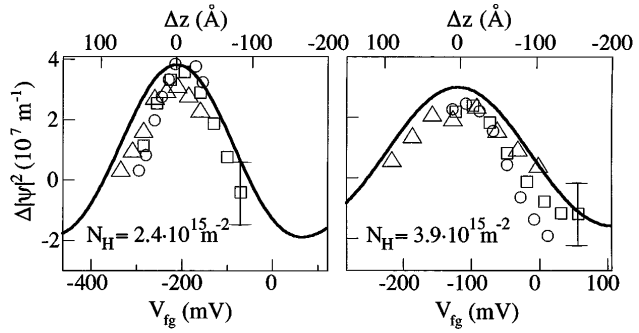

FIG. 3. Measured (symbols) and calculated (solid lines) differences of probability density distributions $\Delta|\psi|^2$ of the two lowest subbands for $N_{\rm H} = 2.4 \times 10^{15}$ m^{-2} and $N_{\rm H} = 3.9 \times 10^{15}$ m^{-2}. The data are obtained by subtracting interpolated values of N_0 from Fig. 2. Triangles correspond to differences from samples with $x = 0.10$ and $x = 0.15$, circles from those with $x = 0.05$ and $x = 0.10$, and squares to $x = 0.05$ and $x = 0.15$. The error bars correspond to an estimated error of 2×10^7 m^{-1}. The front-gate voltages $V_{\rm fg}$ are linearly transformed to positions Δz (upper x axis) according to the experimentally obtained data (Fig. 4).

a function of $V_{\rm fg}$. This displacement is obtained experimentally, analyzing the measured lines of constant $N_{\rm H}$ in the $V_{\rm fg}$-$V_{\rm bg}$ plane (Fig. 1) with a two-capacitor model. The model regards the capacity $C_{\rm fg}$ between the front-gate electrode and the upper edge of the electron gas as being connected in series with the capacity $C_{\rm bg}$ between the lower edge of the electron gas and the back-gate electrode. In this way, the distance between the front-gate electrode and the upper edge of the electron gas can be calculated [13] and thus gives the desired $\Delta z(V_{\rm fg})$. The result for $N_{\rm H} = 3.9 \times 10^{15}$ m^{-2} is shown in Fig. 4 (triangles). As expected, we find an approximately linear relationship $\Delta z(V_{\rm fg})$.

Figure 4(b) shows self-consistently calculated $\Delta|\psi|^2$ for a PBW without a potential perturbation for two different gate voltages. Similar to the experiment, the total carrier density was kept constant when $V_{\rm fg}$ and $V_{\rm bg}$ were varied. In order to obtain $\Delta z(V_{\rm fg})$, the position of maximum $\Delta|\psi|^2$ was traced as a function of $V_{\rm fg}$. The obtained slope of $\Delta z(V_{\rm fg})$ agrees with the experimental data to within 25% (solid line in Fig. 4).

From both experiment and calculations, we find a larger displacement per front-gate voltage at higher electron densities. This is explained by the larger extent of the electron distribution screening the parabolic potential closer to the front-gate electrode. Thus the applied

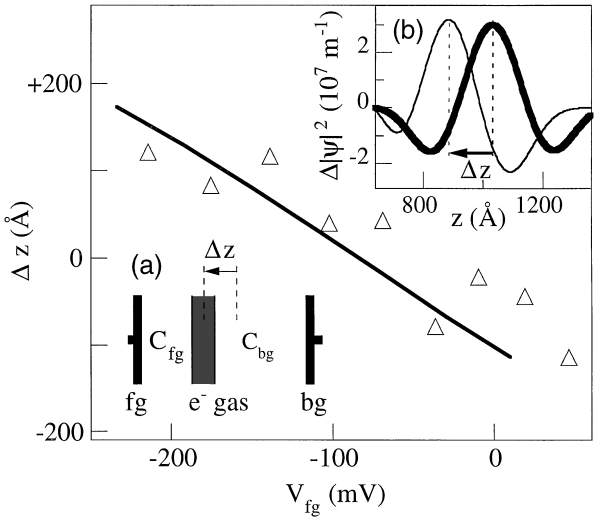

FIG. 4. Relative electron displacement Δz as obtained experimentally (triangles) and from self-consistent calculations (solid line) for $N_{\rm H} = 3.9 \times 10^{15}$ m^{-2}. For the experimental determination of Δz, a two-capacitor model was applied to measured traces of constant $N_{\rm H}$ in the $V_{\rm fg}$-$V_{\rm bg}$ plane (Fig. 1). The model regards two capacities $C_{\rm fg}$ and $C_{\rm bg}$ connected in series (a). The change of the charge on the front-gate electrode (fg) is assumed to be compensated by the change of the charge on the back-gate electrode (bg) while displacing the electron distribution at constant $N_{\rm H}$. The inset (b) shows self-consistently calculated $\Delta|\psi|^2$ at $N_{\rm H} = 3.9 \times 10^{15}$ m^{-2} for two different sets of gate voltages.

voltage drops in a smaller region, and the electric field causing the displacement is increased.

With the obtained $\Delta z(V_{\mathrm{fg}})$, we map the measured $\Delta|\psi|^2$ as a function of spatial coordinate and compare them to the calculated data. The upper axis of Fig. 3 indicates Δz as obtained from the experiment. The solid line corresponds to the calculated $\Delta|\psi|^2$. The data provides clear evidence that differences of single-particle probability densities are measured. With increasing electron density, the screening of the parabola is increased and the wave functions spread out. Simultaneously, the amplitude of the wave functions is reduced due to their normalization. Both features are observed in the presented data (Fig. 3) and are solely due to electron screening of the parabolic potential.

The introduced method is based upon the validity of first-order perturbation theory. Calculations show that in our samples with a three-monolayer thick potential spike, the second-order contribution is at least 5 times smaller than the first order, even for the spike with $x = 0.15$. Experimentally, the accuracy is mainly limited by the measured Hall and subband densities. The main contribution to the error results from deviations in the electron sheet density from N_{H} due to multisubband effects. These are found to be small because the low-field Hall resistance is linear with magnetic field for all measured gate voltages. An upper limit for the error in N_{H} is estimated to be 1×10^{14} m^{-2}, giving an error in N_0 which is about half this value. This corresponds to an error in $\Delta|\psi|^2$ of 2×10^7 m^{-1} (error bars in Fig. 3). Deviations from sample to sample must be considered as well. From our data it can be deduced that they are very small and restricted mainly to small displacements in gate voltages, which are not corrected in our evaluations. Keeping in mind that the four samples were grown on different wafers, this confirms the perfect control of sample growth conditions.

In a perfectly parabolic potential, the shape of the electron distribution is maintained along a line of constant N_{H} in Fig. 1. However, in our samples the parabolic potential is perturbed by the potential spike and by the barriers surrounding the PBW. At a density of 4×10^{15} m^{-2}, the curvature of the investigated parabola corresponds to a rectangular electron distribution of width 510 Å. In our 760 Å wide PBWs, this electron distribution can still be moved ± 125 Å away from the center, without touching the barriers. Quantum mechanically, however, the wave functions reach into the barriers. Thus a displacement of the electron distribution from the center of the PBW will result in small modifications of individual wave functions. Because of its larger spatial extent, ψ_1 is altered more than ψ_0. This leads to modifications of $\Delta|\psi|^2$ far away from the center of the electron distribution, whereas in the center $\Delta|\psi|^2$ remains mainly unaffected. From the self-consistent calculations we estimate the corresponding error in $\Delta|\psi|^2$ to be less than 0.5×10^7 m^{-1} for $\Delta z = \pm 150$ Å and $N_{\mathrm{H}} = 3.9 \times 10^{15}$ m^{-2}. Thus the assumption of a pure displacement of wave functions is reasonable for the investigated range of Δz .

In conclusion, we presented a method to probe locally differences of one-electron probability densities of electrons in a screened potential well. This has been done in a transport experiment at different electron sheet densities. Although, in principle, the method can be applied to any kind of potential well using a large number of samples, in the special case of a PBW, the spatial distribution of probability density differences can be mapped out with only two samples. We have demonstrated that in PBWs, the spatial distribution can be scanned by displacing the wave functions without changing their shape. Our experimental results are in excellent agreement with self-consistent subband calculations.

We gratefully acknowledge fruitful discussions with W. Zwerger, T. Heinzel, and T. Ihn. The self-consistent calculations were performed using a computer program written by G. Snider. This project was financially supported by the Swiss Science Foundation and AFOSR Grant No. F-49620-94-1-0158.

[1] M. F. Crommie, C. P. Lutz, and D. M. Eigler, Science **262**, 218 (1993).
[2] J.-Y. Marzin and J.-M. Gérard, Phys. Rev. Lett. **62**, 2172 (1989).
[3] T. C. Hsieh, T. Miller, and T.-C. Chiang, Phys. Rev. Lett. **55**, 2483 (1985).
[4] M. Sundaram, A. C. Gossard, J. H. English, and R. M. Westervelt, Superlattices Microstruct. **4**, 683 (1988).
[5] M. Shayegan, T. Sajoto, M. Santos, and C. Silvestre, Appl. Phys. Lett. **53**, 791 (1988).
[6] K. Ensslin, A. Wixforth, M. Sundaram, P. F. Hopkins, J. H. English, and A. C. Gossard, Phys. Rev. B **47**, 136 (1993).
[7] K. Karrai, H. D. Drew, M. W. Lee, and M. Shayegan, Phys. Rev. B **39**, 1426 (1989).
[8] A. Wixforth, M. Sundaram, K. Ensslin, J. H. English, and A. C. Gossard, Phys. Rev. B **43**, 10 000 (1991).
[9] L. Brey, N. F. Johnson, and B. I. Halperin, Phys. Rev. B **40**, 10 647 (1989).
[10] M. Hartung, A. Wixforth, K. L. Campmann, and A. C. Gossard, Superlattices Microstruct. **19**, 1 (1996).
[11] A. C. Gossard, IEEE J. Quantum Electron. **22**, 1649 (1986).
[12] K. D. Maranowski, J. P. Ibbetson, K. L. Campman, and A. C. Gossard, Appl. Phys. Lett. **66**, 3459 (1995).
[13] Details will be discussed elsewhere.